Journal of Sound and Vibration (2002) **257**(2), 247–264
doi:10.1006/jsvi.5056, available online at http://www.idealibrary.com on IDEAL®

HEALTH-MONITORING METHOD FOR BRIDGES UNDER ORDINARY TRAFFIC LOADINGS

J. W. Lee and J. D. Kim

Department of Structural Systems Engineering, Korea Institute of Machinery and Materials, Yusong-ku, Taejon 305-600, *Korea. E-mail: jwlee@kimm.re.kr*

and

C. B. Yun, J. H. Yi and J. M. Shim

Department of Civil Engineering, Korea Advanced Institute of Science and Technology, Yusong-ku, Taejon 305-701, *Korea. E-mail: ycb@kaist.ac.kr*

(*Received* 2 *April* 2001, *and in final form* 11 *December* 2001)

A method for damage estimation of a bridge structure is presented using ambient vibration data caused by the traffic loadings. The procedure consists of identification of the operational modal properties and the assessment of damage locations and severities. An experimental study is carried out on a bridge model with a composite cross-section subjected to vehicle loadings. Vertical accelerations of the bridge deck are measured while vehicles are running. The modal parameters are identified from the free-decay signals extracted using the random decrement method. The damage assessment is carried out based on the estimated modal parameters using the neural networks technique. As input to the neural networks, the ratios of the resonant frequencies between before and after damages and the mode shapes after the damages are used to take into account the mass effect of the traffic on the bridge. The identified damage locations and severities agree reasonably well with the inflicted damages on the structure.

1. INTRODUCTION

Bridges constitute an important part of the national infrastructures. Preventive maintenance and structural safety of bridges may be guaranteed by the application of health-monitoring systems, which can provide valuable information for detailed inspection, repair and rehabilitation of bridges. Structural identification technique from ambient vibration data is essential particularly for on-line monitoring.

In this study, random decrement (RD) technique [1] is used to estimate free-decay signals (i.e., randomdec signatures) from the ambient vibration data induced by unmeasured traffic loadings. The properties of the operational modes are extracted from the randomdec signatures. Inverse modal perturbation technique [2] is applied to update the baseline finite element (FE) model based on the impact test results. Then, neural networks technique [3] is used to estimate the damage locations and severities based on the modal properties obtained from the vehicle tests. The procedure for bridge monitoring presented in this study is summarized in Figure 1.

A simply supported bridge model with a composite cross-section was built, and traffic loadings were simulated using three model vehicles connected to each other. Vertical accelerations of the bridge were measured at several locations, while the vehicles are

0022-460X/02/$35.00

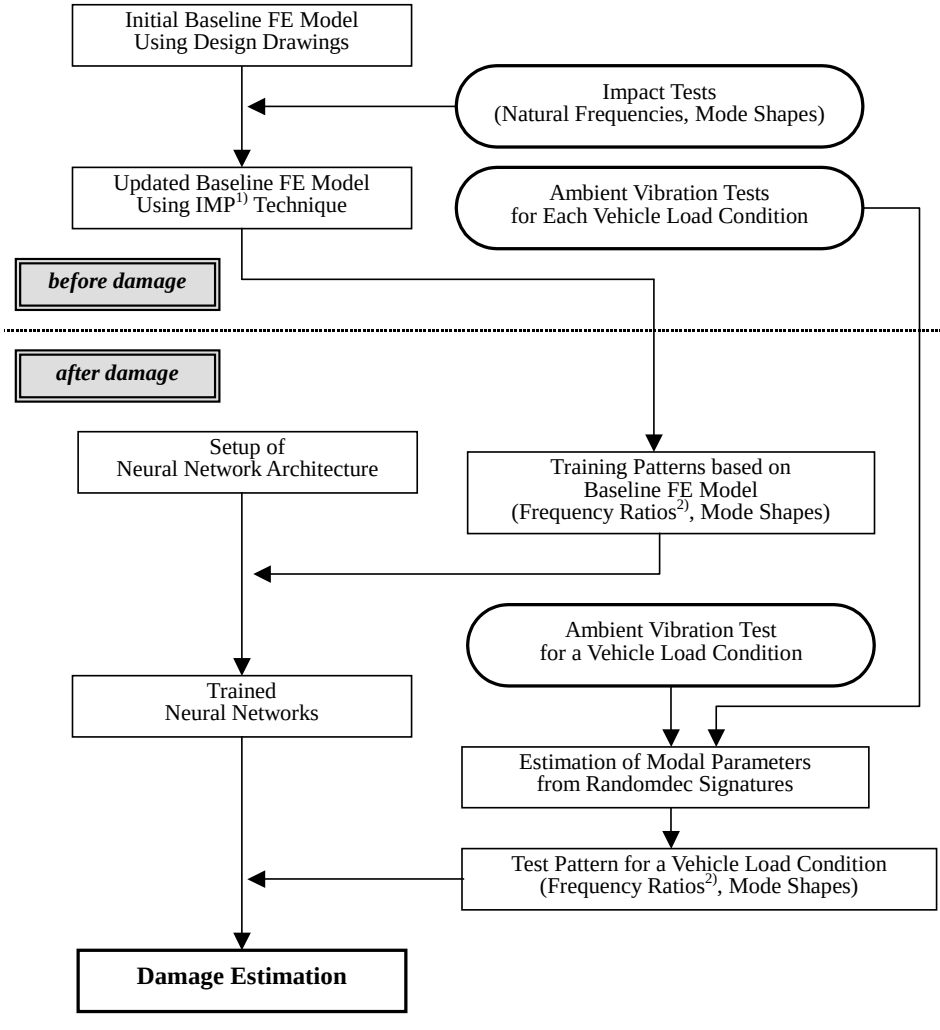

Figure 1. Schematic of bridge monitoring procedure: (1) IMP: inverse modal perturbation; (2) frequency ratios: between before and after damages.

running. A series of element-level damages was inflicted on the structure, and travelling tests were carried out for each damage case with varying the weight of vehicles. Resonant frequencies for the vehicle tests were estimated differently in accordance with the weight of vehicles. Therefore, the ratios of the resonant frequencies between before and after the damages under a same vehicle load condition and the mode shapes after the damages were used as input data to the neural networks. The estimated damage locations and severities are found to compare well with the inflicted damages.

2. THEORETICAL BACKGROUND

2.1. RANDOM DECREMENT TECHNIQUE

The fundamental concept of the RD technique [1, 4, 5] is based on the fact that the random response of a structure is composed of two parts: i.e., a deterministic part and

a random part. Since the introduction of the RD technique, it has been used for identification of various types of structures such as bridges, offshore platforms, aeroplanes, etc. [4, 6–9]. By averaging enough sample responses with a prescribed initial condition, the random part associated with the random excitation will average out, leaving the deterministic part. It has been shown that the deterministic part that remains is the free-decay response associated with the initial condition, from which the modal parameters and the damping characteristics can be easily extracted. The RD signature vector $\mathbf{z}(\tau, x)$ can be obtained as

$$\mathbf{z}(\tau, x) = \frac{1}{N} \sum_{i=1}^{N} \mathbf{y}(\tau + t_i, x), \tag{1}$$

where $\mathbf{y}(t, x)$ is the measurement at x, t_i's are the time instances satisfying a prescribed triggering condition at a leading station, N is the number of the triggering points, and τ is the time variable.

2.2. NEURAL NETWORKS TECHNIQUE

A popular neural networks model called a multi-layer perception neural networks [3] is used for identification of the element-level stiffness parameters. The neural networks employed in this study consist of an input layer, two hidden layers, and an output layer. The input layer contains the measured modal properties, and the output layer consists of the element stiffness indices to be identified. The input/output relationship of the neural networks can be non-linear as well as linear, and its characteristics are determined by the synaptic weights assigned to the connections between the neurons in two adjacent layers. The systematic way of updating the weights to achieve a desired input/output relationship based on a set of training patterns is referred to as training or learning algorithm. In this study, the standard back-propagation algorithm [3, 10, 11] is used, and the noise injection learning (NIL) [12] is also employed to reduce the effects of measurement noise. In NIL algorithm, the training is carried out using the artificially contaminated training patterns with noise of a prescribed level. The generalization capability of the neural networks can be remarkably enforced through this algorithm, because this algorithm has similar effect to the regularization technique that is used to mollify the ill-posedness of the inverse problems [12, 13].

3. DESCRIPTION OF EXPERIMENTS

3.1. BRIDGE MODEL AND EXPERIMENTAL SET-UP

A simply supported single-span bridge was built to verify the present method for structural identification. A schematic of the experimental set-up is shown in Figure 2. The bridge model has a composite cross-section with two steel girders and a concrete slab as shown in Figure 3. The span length is 6 m and the total weight is 1030 kgf. Three test vehicles connected to each other by wires were used as in Figure 2. The weights of the empty vehicles are 10, 20 and 20 kgf, respectively, and can be made heavier by adding extra weights on the vehicles. Two bumps were placed at the 1/4 and the 2/3 points of the bridge span from the left support. The bumps were attached to the slab surface to simulate the impact forces by the vehicles due to the roadway roughness. The shape of the bump is triangular, of which height and width are 1 and 15 cm, respectively, while the diameter of the wheel is 15 cm.

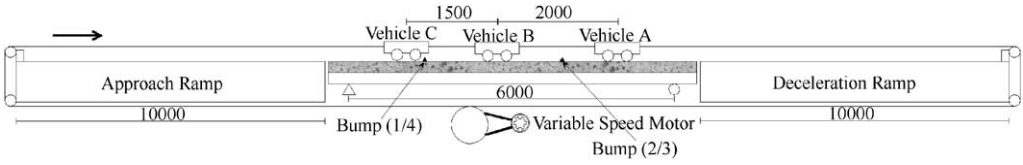

Figure 2. Schematic of experimental set-up (lengths in mm).

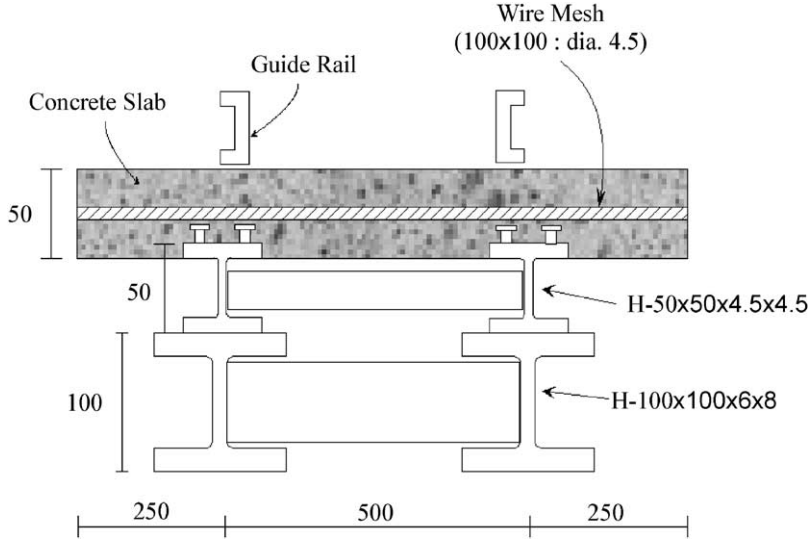

Figure 3. Section view of the bridge model (lengths in mm).

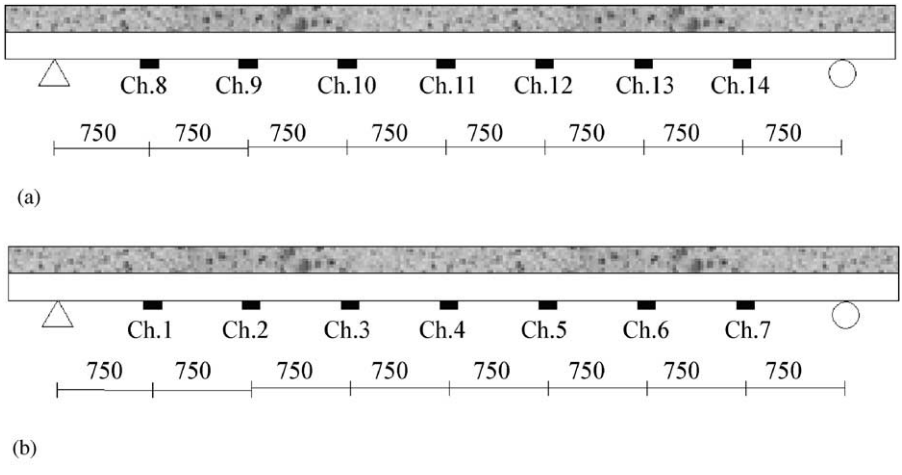

Figure 4. Measurement locations (lengths in mm): (a) left girder; and (b) right girder.

The vehicles are pulled along the bridge by a wire rope and travel inside of two guide rails, and the vertical vibration of the bridge is measured along the girders. Seven accelerometers are attached to the bottom flange of each girder (H—$100 \times 100 \times 6 \times 8$) as in

Figure 4. Two sets of the measured data on two girders are used to acquire more reliable data by averaging and to discern the bending modes from the torsion modes.

3.2. TEST PROCEDURE AND VEHICLE SPEED

Vehicle tests were performed 20 times for each of eight damage cases shown in Table 1. The FE model of the bridge and the element numbers are shown in Figure 5. For Intact Case and Damage Cases 1 and 2, tests were carried out 20 times under each of five vehicle load conditions described in Table 1. The load conditions were varied by changing the weights of the vehicles in order to investigate the mass effect of the vehicles.

Damages were inflicted by cutting out parts of the bottom flanges of the girders (H—$100 \times 100 \times 6 \times 8$). The data were sampled at 1 kHz for 30 s during a round-trip of the vehicles. A round-trip consists of forward and backward trips by the vehicles. At first, three vehicles were pulled forward. Then, after all vehicles passed through the bridge and the vibration completely subsided, the vehicles were pulled backward. The net duration for the vehicles on the bridge was about 5 s for each one-way trip (refer to Figure 6). Impact load tests were also carried out for each damage case and vehicle load condition for the purpose of comparison.

In this study, the speed of the model vehicles (v_m) for damage estimation is taken as 2·0 m/s, of which the equivalent vehicle speed for the prototype structure (v_p) is 18·4 km/h. The equivalent speed (v_p) is calculated using the following similarity relationship for the ratio of the nominal exciting frequency by the vehicles (v/l) to the first resonant frequency of the bridge (f):

$$\frac{(v_p/l_p)}{f_p} = \frac{(v_m/l_m)}{f_m} \tag{2}$$

TABLE 1

Damage scenarios

	Loss of bending rigidity (%)			Weight of vehicle (kgf)			Total weight of vehicles (kgf)
	Element 3	Element 5	Element 7	Vehicle A	Vehicle B	Vehicle C	
Case 1	—	− 16·6	—	—	20	—	20
				10	20	20	50
				40	20	40	100
				80	40	80	200
				120	60	120	300
Case 2	—	− 16·6	− 9·5	—	20	—	20
				10	20	20	50
				40	20	40	100
				80	40	80	200
				120	60	120	300
Case 3	—	− 16·6	− 16·9	80	40	80	200
Case 4	—	− 16·6	− 25·4	80	40	80	200
Case 5	− 15·8	− 16·6	− 25·4	80	40	80	200
Case 6	− 15·8	− 31·0	− 25·4	80	40	80	200
Case 7	− 22·1	− 31·0	− 25·4	80	40	80	200
Case 8	− 32·1	− 31·0	− 25·4	80	40	80	200

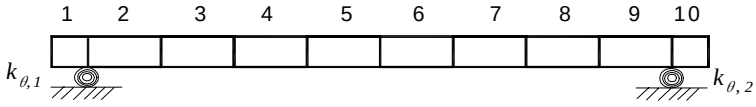

Figure 5. FE model and element numbers.

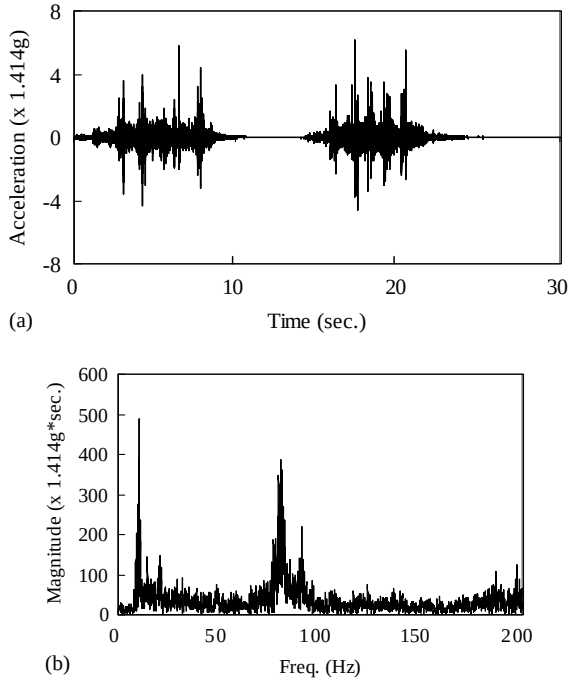

Figure 6. Acceleration time history at Ch.11 and its Fourier amplitude spectrum: (a) time history; and (b) Fourier amplitude spectrum.

where v is the vehicle speed, l is the span length, and subscripts p and m indicate the prototype and model respectively. Assuming that the prototype structure has l_p and f_p values 50 m and 3·5 Hz, and considering that the model structure has l_m and f_m values 6 m and 11·4 Hz and v_m is 2·0 m/s, the corresponding vehicle speed in the prototype case (v_p) is 18·4 km/h. The above speed is much slower than the ordinary traffic speed. But higher speed was not able to be simulated because of the capacity of the pulling motor particularly with the heavy weight of vehicles and the insufficient lengths of the acceleration and deceleration ramps due to the limited space of the laboratory.

To investigate the effects of the vehicle speed to the operational modes, preliminary tests were carried out on the bridge model with smaller girders (H—$50 \times 50 \times 4{\cdot}5 \times 4{\cdot}5$) for speeds of 2·0, 2·5, and 3·0 m/s with one test vehicle (60 kgf). Based on equation (2), the corresponding vehicle speeds for the prototype structure are 36·1, 45·1, and 54·1 km/h respectively (note: $f_m = 5{\cdot}82$ Hz). The operational modal properties were estimated for each speed for the four lowest modes using the technique described in the next section. The discrepancies between the resonant frequencies for different speeds are found to be less than 0·7% and the modal assurance criteria (MAC) between the mode shapes for different speeds are greater than 0·9911 as shown in Tables A1 and A2 in Appendix A. The results strongly indicate that the properties of the operational modes are barely influenced by the vehicle

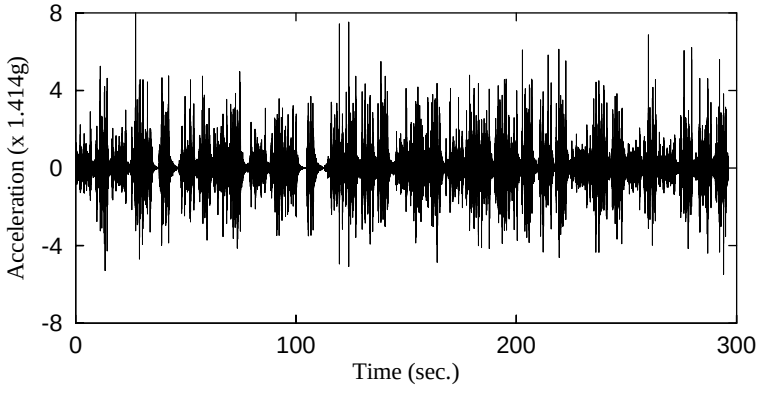

Figure 7. Randomly compounded time history at Ch. 11.

speed. In reference [14], similar tests were performed on a bridge model with two continuous span aluminum plate girders and a total length of 4·57 m. The effects of vehicle speed were evaluated for 0·3, 0·6, 1·2, and 2·4 m/s of the model vehicles. It was concluded that the resonant frequencies and shapes of the operational modes are not influenced by vehicle speed.

4. MODAL PARAMETER ESTIMATION

4.1. DATA ANALYSIS FOR RANDOMDEC SIGNATURES

Vehicle tests were performed for 20 round trips. A typical acceleration time history and its Fourier amplitude spectrum acquired for a round-trip of the vehicles are shown in Figure 6. The noise content appears to be very high. Forty sets of the one-way vibration responses were compounded with random arrival times to generate a compounded time history. Ten different sets of the compounded time histories were generated in the same manner but with different arrival times. An example of a randomly compounded acceleration time history in Ch. 11 is shown in Figure 7. The randomdec signatures were calculated from each set of the compounded time histories using a triggering condition of zero crossing with a positive slope at the leading station, which was taken as the center of the span for the first and third modes, the quarter point for the second mode, and the 1/8 point for the fourth mode respectively. A randomdec signature obtained in Ch. 11 and its Fourier amplitude spectrum are shown in Figure 8. The resonant frequencies and mode shapes are determined from the cross-spectral density functions of the randomdec signatures.

4.2. ESTIMATED MODAL PROPERTIES

The identified resonant frequencies for the baseline (i.e., intact) case from the vehicle tests are compared with those obtained from the impact load tests in Table 2. The estimated frequencies for the vehicle tests are found to be smaller than the others due to the mass effect of the moving vehicles, which is very difficult to evaluate analytically. Table 2 also shows the frequencies estimated from the tail portions of the vibration data which correspond to the free vibration responses after all the vehicles passed the bridge section. The results are found to be very close to the impact test results. However, a method using the whole length of the vibration data as in Figure 6 is more convenient for the purpose of bridge monitoring.

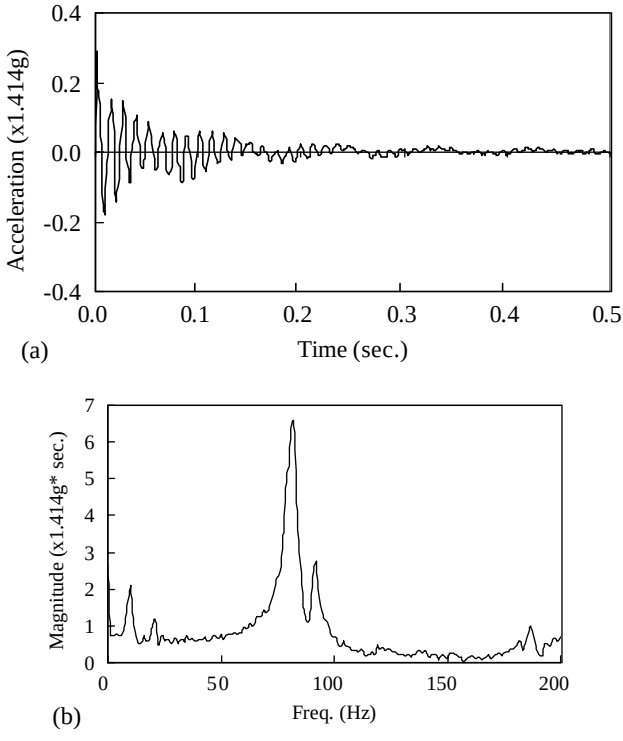

Figure 8. Randomdec signature at Ch. 11 and its Fourier amplitude spectrum: (a) randomdec signature; and (b) Fourier amplitude spectrum.

TABLE 2

Resonant frequencies of intact case (Hz)

	Tests		Analysis	
Modes	Impact	Vehicle	Initial model	Updated model
1	11·40	10·43 (11·29)	9·23	11·45
2	41·00	40·47 (41·36)	36·87	40·09
3	81·80	81·37 (82·20)	82·69	84·13
4	137·4	137·6 (137·5)	145·9	146·7

Note 1: The values for the vehicle test are obtained when the total weight of vehicles is 200 kgf.
Note 2: The values in parentheses are obtained using the tail portions of the responses.

Figure 9 compares the mode shapes obtained from the vehicle tests (total weight of vehicles: 200 kgf), and the impact load tests. Two sets of the mode shapes are found to be in good agreement, which indicates that the mode shapes remain almost the same regardless of the moving vehicle masses on the bridge.

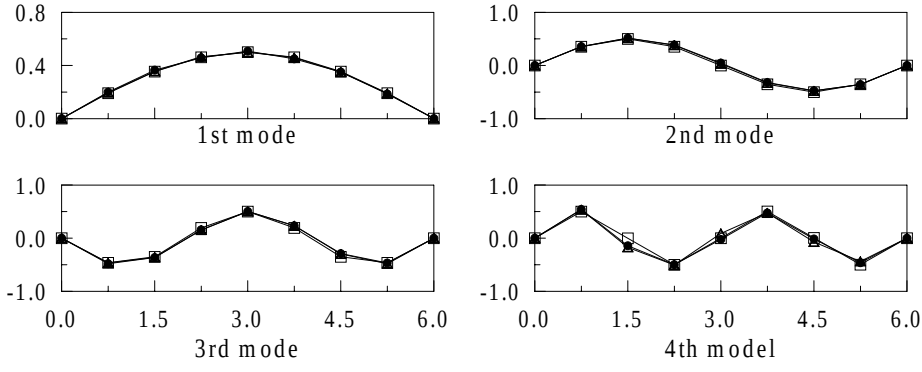

Figure 9. Mode shapes of intact structure: ●, impact test; △, vehicle test; □, updated FE analysis.

4.3. UPDATING OF BASELINE FINITE ELEMENT MODEL

A finite element (FE) model is constructed for the bridge to verify the proposed modal parameter estimation method and to establish the baseline FE model for the subsequent damage assessment. The bridge with a composite section is modelled using equivalent beam elements as in Figure 5. The bending rigidity of the girder section, $(EI)_e^I$ is initially evaluated from the dimension of the section as $6{\cdot}34 \times 10^6\,\mathrm{N\,m^2}$. In the FE model, the effects of the configurations of the supports (Figure 10), such as the offset between the rigidity center of the section and the support, are represented by rotational spring elements, $k_{\theta,1}$ and $k_{\theta,2}$. The bending rigidity of each segment of the girder and the rotational spring constants at the supports are updated by using the inverse modal perturbation technique [2] based on the impact test results. For the purpose of model updating, the following stiffness indices are employed:

$$\alpha_e = \frac{(EI)_e^0}{(EI)_e^I} \quad \text{and} \quad \alpha_{\theta,j} = \frac{k_{\theta,j}^0}{k_{\theta,j}^0 + k_{\theta,j}^I}, \tag{3}$$

where superscripts "I" and "0" denote the initial and updated intact cases, respectively, and $k_{\theta,j}^I$ is approximately taken as $3(EI)_e^I/L$ ($= 3{\cdot}17 \times 10^6$ N m) with L being the span length of the bridge.

The updated stiffness properties are shown in Table 3. The updated stiffness indices of elements 1, 2, 5, 6, 9, and 10 are found to be different from those of elements 3, 4, 7, and 8. It is due to the fact that the bending rigidity of the composite section is not exactly uniform along the longitudinal direction due to the imperfection during fabrication and the cracks in the transverse direction in the concrete slab in the middle and near the supports occurred during series of erections and removals of the bridge model. The modal properties of the updated model are compared with the measured ones in Table 2 and Figure 9. The errors in the resonant frequencies of the updated model are found to be very small for the first two modes. However, the errors are 3 and 7% for the third and fourth modes respectively. The errors for the latter two frequencies are due to the simple equivalent beam model for the bridge. Furthermore, the updating was carried out by assigning larger weights (10 times) to the first two modes.

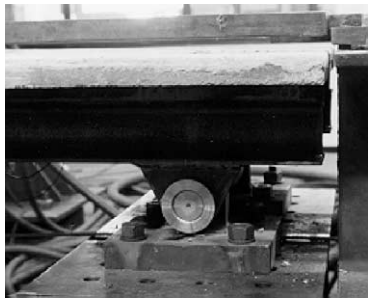

Figure 10. Boundary condition at a support.

TABLE 3

Updated stiffness indices for intact case (α_c *and* α_θ)

Element numbers	1	2	3	4	5	6	7	8	9	10	$\alpha_{\theta,1}$	$\alpha_{\theta,2}$
Stiffness indices (α_e and α_θ)	0·8	0·8	1·1	1·1	0·8	0·8	1·1	1·1	0·8	0·8	0·39	0·39

5. DAMAGE ESTIMATION

5.1. ELEMENT STIFFNESS INDEX AND DAMAGE SEVERITY

For the purpose of damage estimation, the element stiffness index (α_j) and the element damage severity (d_j) for the jth element are defined as

$$\alpha_j = \frac{(EI)_j^d}{(EI)_j^0} \quad \text{and} \quad d_j = 1 - \alpha_j, \tag{4}$$

where superscripts "0" and "d" indicate the intact and damaged states.

5.2. MODAL PROPERTIES AS INPUT TO NEURAL NETWORKS

The stiffness indices of eight beam elements are estimated for each damage case using neural networks technique based on the modal properties obtained from the vehicle tests. The ratios of the resonant frequencies between before and after damages for a same traffic load condition and the mode shapes after the damages are used as input data to the neural networks (Figure 11), since the resonant frequencies vary if the vehicle masses are included while the mode shapes remain almost the same as in Figure 9. The modal properties for the first four modes are used, which results in 32 nodes in the input layer. Two hidden layers with 20 and 10 nodes each are introduced. The neural networks are trained using the modal data simulated from the cases without moving vehicles, since it is very difficult to analytically obtain the modal properties of the bridge with moving vehicles. The basis of using the frequency ratios obtained from the cases without moving vehicles is elaborated below.

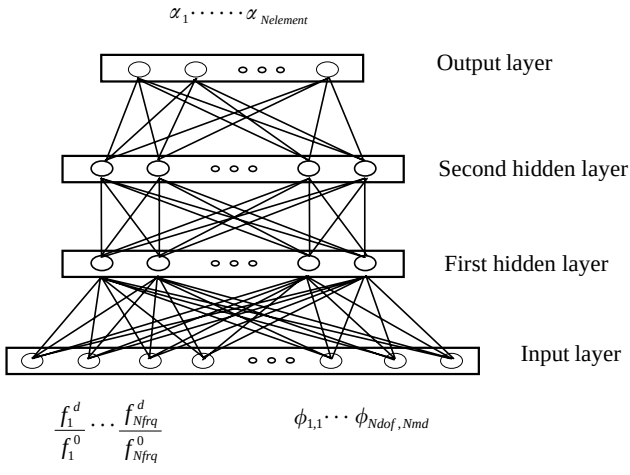

Figure 11. Structure of neural networks.

For the purpose of bridge monitoring, a reasonable criterion for the traffic load condition may be established to a reasonable number of cases depending on the types and sizes of the bridge and traffic such as very heavy, heavy, medium, light, and very light conditions. The traffic condition may be monitored by weight in motion (WIM) system, CCTV, etc. The resonant frequencies for the intact case can be predetermined for each load condition. Then for a traffic load condition V_l on the bridge, the ratio of the ith resonant frequencies can be written as

$$\frac{f_{S+V_l,i}^{d^2}}{f_{S+V_l,i}^{0\ 2}} = \frac{\kappa_{S+V_l,i}^d/\mu_{S+V_l,i}^d}{\kappa_{S+V_l,i}^0/\mu_{S+V_l,i}^0} = \frac{\kappa_{S+V_l,i}^d/\kappa_{S+V_l,i}^0}{\mu_{S+V_l,i}^d/\mu_{S+V_l,i}^0} \approx \frac{\kappa_{S+V_l,i}^d}{\kappa_{S+V_l,i}^0} \approx \frac{\kappa_{S,i}^d}{\kappa_{S,i}^0}, \tag{5}$$

where the subscripts "S" and "V" denote the structure (bridge) and vehicle respectively. κ_i and μ_i are modal stiffness and modal mass for the ith mode respectively. The approximation for the second last term is based on the fact that the change in the modal mass due to damage is much smaller than the change in the modal stiffness. On the other hand, the approximation for the last term is from the fact that the mode shapes remain almost same as those of the case without the moving vehicles on the bridge as shown in Figure 9.

For a case without vehicle load, the ratio of the resonant frequencies between before and after damage can be obtained similarly as

$$\frac{f_{S,i}^{d^2}}{f_{S,i}^{0^2}} = \frac{\kappa_{S,i}^d/\mu_{S,i}^d}{\kappa_{S,i}^0/\mu_{S,i}^0} = \frac{\kappa_{S,i}^d/\kappa_{S,i}^0}{\mu_{S,i}^d/\mu_{S,i}^0} \approx \frac{\kappa_{S,i}^d}{\kappa_{S,i}^0} \tag{6}$$

Finally, the following relationship can be obtained for each vehicle load condition V_l and the ith mode from equations (5) and (6) as

$$\frac{f_{S+V_l,i}^d}{f_{S+V_l,i}^0} \approx \frac{f_{S,i}^d}{f_{S,i}^0} \tag{7}$$

Verification for the approximate relationship in equation (7) has been carried out for Damage Cases 1 and 2 with various total weight of vehicles, i.e., 20, 50, 100, 200 and 300 kgf as shown in Table 1. The load conditions may be considered as very light to heavy

TABLE 4

Frequency ratios between before and after damages for various vehicle load conditions

Damage Cases	Modes	No vehicle (impact test)	Total vehicle weights (kgf) 20	50	100	200	300	Average and relative error
1	1	0·932	0·935	0·932	0·932	0·945	0·945	0·938 (0·64)
	2	0·977	0·992	0·977	0·992	0·995	0·978	0·987 (1·02)
	3	0·954	0·953	0·954	0·955	0·954	0·954	0·954 (0·00)
	4	0·966	0·966	0·966	0·966	0·966	0·967	0·966 (0·00)
2	1	0·918	0·918	0·917	0·918	0·918	0·920	0·918 (0·00)
	2	0·945	0·947	0·945	0·944	0·946	0·944	0·945 (0·00)
	3	0·950	0·959	0·949	0·963	0·950	0·951	0·955 (0·53)
	4	0·945	0·946	0·949	0·944	0·945	0·945	0·946 (0·11)

Note: The values in parentheses are errors in %.

conditions, since the live to dead load ratios are in the range 0·02–0·29. Table 4 shows the frequency ratios between before and after damages for various moving vehicle load conditions. Frequency ratios of the first four modes for five different load conditions are found to be very close to those ratios without moving vehicles. The differences between the frequency ratios with and without the moving vehicles are less than 2%, which indicates the validity of the approximation in equation (7).

The accuracy of the damage estimation can be deteriorated, if one picks up wrong traffic conditions in applying equation (7). For reliable damage estimation, dual health-monitoring systems may be utilized: one based on the resonant frequencies and the mode shapes, and the other based on the mode shapes only which remain almost same regardless of the moving vehicle masses on the bridge. The results in the next section show that the neural networks based on the mode shape data only also gives reasonable estimates for damages. If the monitoring system gives an indication of occurrence of damages, verification analysis can be quickly carried out several times, since the damage estimation using the neural networks takes very short time. Hence, the error due to the wrong pick-up of the traffic condition may not cause serious problem. The present method is developed on the basis of the averaging effects of each vehicle dynamics. Hence, the reliability of the damage estimation may be better with the moderate size traffic which may provide enough vibration amplitudes and enough number of cars for averaging.

5.3. ESTIMATION OF ELEMENT DAMAGE SEVERITIES

The element-level damage locations and severities are estimated using the neural networks technique for various cases described in Table 1. Ten thousand training patterns were generated around the updated (intact) FE model, and training was carried out for 300 epochs to obtain a stable estimation error. The element stiffness indices (refer to equation (4)) were randomly sampled in the range 0·5–1·5 using the Latin hypercube sampling technique [15]. It was reported that the multi-layered neural networks can be well trained for the practical application, if the number of training patterns is over 10 times of the total number of synapses [16]. The total number of synapses employed in this study is 920. Hence, 10 000 training patterns are judged to be appropriate.

TABLE 5

Resonant frequencies for various damage cases (Hz)

Modes	1	2	3	4
Intact	10·43	40·47	81·37	137·6
Case 1	10·10	40·20	79·70	136·0
Case 2	9·80	40·10	78·80	136·0
Case 3	9·70	38·67	77·70	135·0
Case 4	9·63	38·50	77·83	134·1
Case 5	9·43	37·20	76·60	132·4
Case 6	8·93	35·63	71·40	130·2
Case 7	8·90	35·37	70·00	130·4
Case 8	8·57	34·90	67·80	130·1

Note: The values are obtained when the total weight of vehicles is 200 kgf.

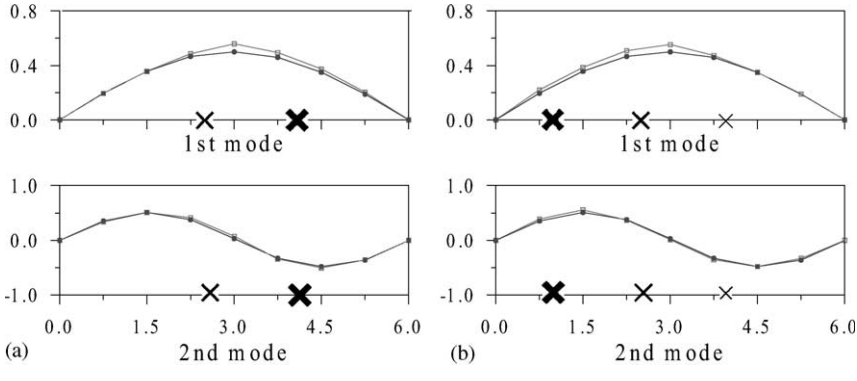

Figure 12. Mode shapes for damage cases: (a) Damage Case 4; (b) Damage Case 8.—●—, intact case; —□—, damage case; (✖), large damage; (✖), medium damage; (×) small damage.

Table 5 shows the resonant frequencies obtained from the vehicle tests for eight damage cases. It can be found that the resonant frequencies decrease as damages become severer. Figure 12 shows the changes of the mode shapes due to various levels of damages for Damage Cases 4 and 8.

The damage identifications were carried out incorporating the noise injection learning (NIL) algorithm to consider the errors in the input modal data, which may cover the modelling error and the identification error of the modal properties. The levels of the noises considered in the NIL are 5% for the first and second resonant frequencies, 10% for the third and fourth resonant frequencies, and 10% for mode shapes. The noise levels were determined based on the modelling error in the updated model and the measurement noise.

The estimated damage severities for Damage Cases 1 and 2 with various vehicle load conditions are shown in Figure 13. It can be found that the damage locations and severities are very well estimated for all vehicle load conditions.

Figure 14 shows the inflicted and estimated damage severities for eight damage cases with the total vehicle weight of 200 kgf. The results with the NIL algorithm are compared to those without the NIL algorithm. It can be found that the accuracy of the estimation is remarkably improved if the NIL has been carried out. In Damage Case 5, an intact element

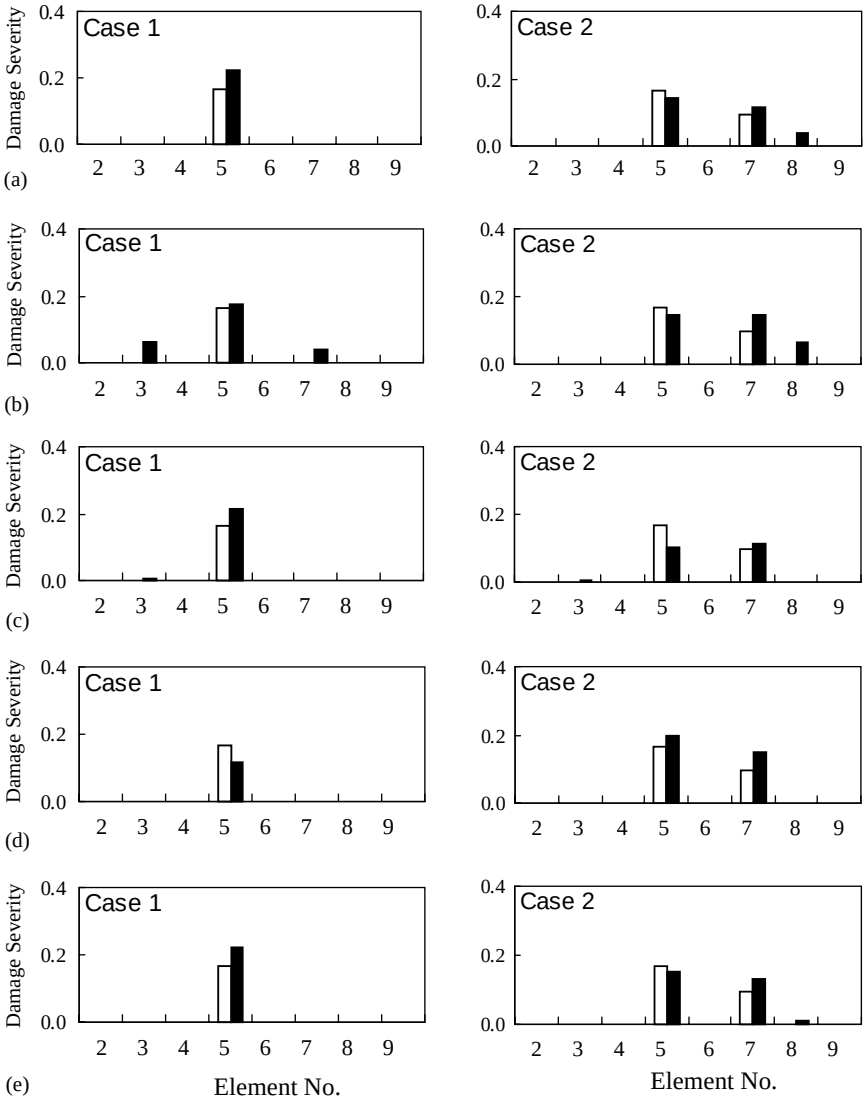

Figure 13. Estimated damage severity for various total weights of vehicles (damage cases 1 and 2). (a) 20 kgf; (b) 50 kgf; (c) 100 kgf; (d) 200 kgf; and (e) 300 kgf. □, inflicted; ■, Estimated w/ NIL.

(No. 8) is estimated as a damaged one, while the damage severity for one of three damaged elements (No. 5) is very much under-estimated. But, in the other damage cases, all of the inflicted damages are detected very successfully. However, the degree of damage severity generally tends to be slightly overestimated.

For the purpose of comparison, damage estimation was also carried out using the neural networks trained with the mode shape data excluding the information on the resonant frequencies, since the frequencies vary with the masses of the moving vehicles. In Figure 15, the results for eight damage cases are shown along with those obtained using the mode shapes and the frequency ratios before and after the damages occur. The accuracy of the estimates is found to be still reasonable, but considerably deteriorated compared to those estimated using both of the mode shapes and the resonant frequency ratios. This result

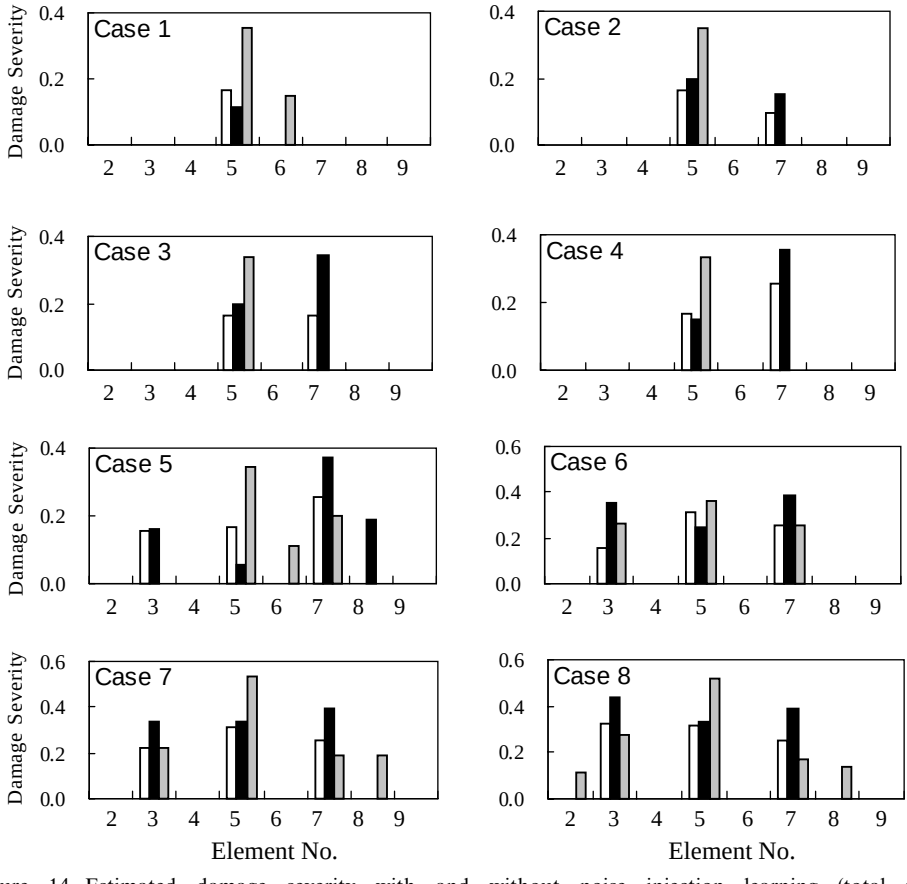

Figure 14. Estimated damage severity with and without noise injection learning (total vehicle weight = 200 kgf). □, inflicted; ■, estimated w/NIL; ▨, estimated w/o NIL.

indicates the usefulness of the frequency ratios between before and after damages instead of the frequencies themselves, as input components to the neural networks for damage identification.

6. CONCLUDING REMARKS

A method is presented for the element-level damage assessment of bridge using the modal properties obtained from the vibration data caused by ordinary traffic loadings, and verified by a series of vehicle tests on a bridge model. It has been found that the free-decay responses can be reasonably identified from the ambient vibration data using the random decrement method, and the modal parameters can be easily estimated thereafter.

Updating of the FE model for the intact structure is carried out to establish the baseline model using the inverse modal perturbation technique. Then damage estimation is performed for various cases with inflicted damages using the neural networks technique incorporating the noise injection learning technique. The frequency ratios between before and after damages and the mode shapes after the damages are used as inputs to the neural networks. The frequency ratios have been used instead of the frequencies, since the resonant frequencies of the bridge extracted from the vibration data vary depending on the mass of the moving vehicles. It has been found that most of the inflicted damages can be detected

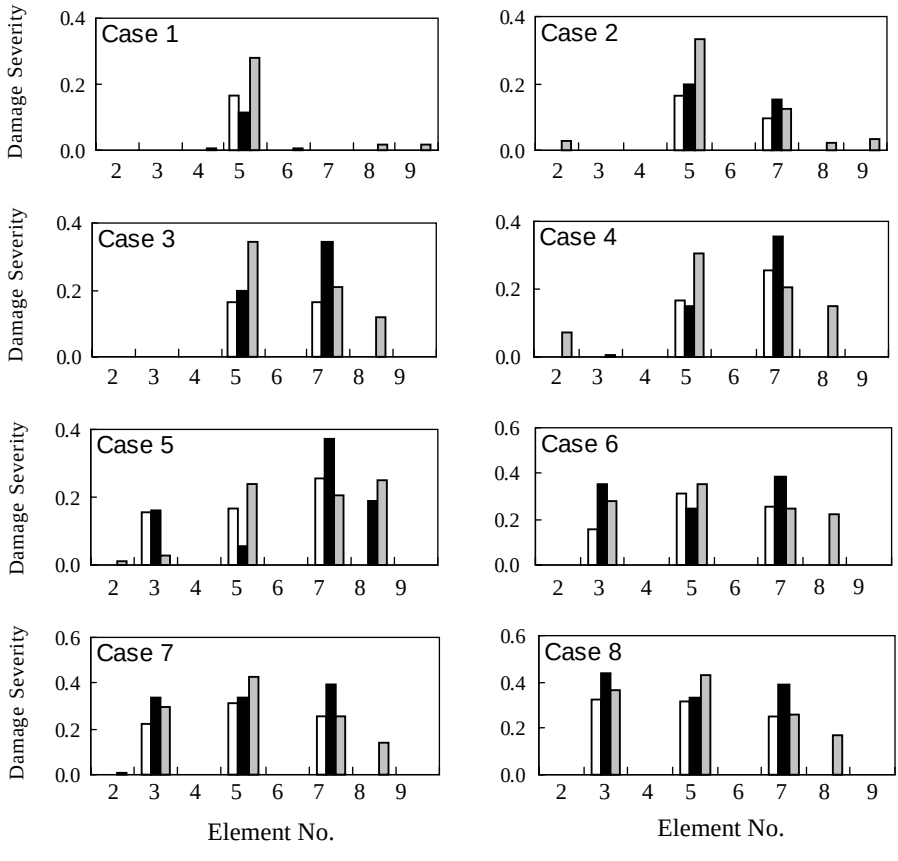

Figure 15. Estimated damage severity with and without the frequency data (total vehicle weight = 200 kgf). □, Inflicted; ■, using frequencies and modes; ▨, using modes only.

very successfully for various vehicle load conditions; however, the degree of damage severity generally tends to be slightly overestimated. For practical application, the accuracy of the estimated damage severities may be less important, as long as the damage locations can be detected precisely.

ACKNOWLEDGMENTS

This study was supported by the Critical Technology Project sponsored by the Ministry of Science and Technology and a National Research Laboratory Project entitled "Aseismic Control of Structures" sponsored by the Korea Institute of Science & Technology Evaluation and Planning. Their financial support is greatly acknowledged.

REFERENCES

1. H. A. COLE 1968 *AIAA Paper*, no. 68-288. On-the-line analysis of random vibrations.
2. C. B. YUN and K. S. HONG 1992 *Proceedings of the 4th East Asia-Pacific Conference on Structural Engineering and Construction, Seoul, Korea.* Damage assessment of structures by inverse modal perturbation method.

3. S. HAYKIN 1994 *Neural Networks—a Comprehensive Foundation*. New York: Macmillan.
4. J. C. S. YANG, J. CHEN and DAGALAKIS 1985 *Journal of Energy Resources Technology*, *American Society of Mechanical Engineers* **106**, 38–42. Damage detection in offshore structures by the random decremental technique.
5. J. C. ASMUSSEN and R. BRINCKER 1996 *Proceedings of* 14*th International Modal Analysis Conference*, *Dearborn*, *MI*, 246–252. Estimation of frequency response functions by random decrement.
6. S. R. IBRAHIM 1979 *The Shock and Vibration Bulletin*. **49** (Part 2 of 3), 165–170. Application of random time domain analysis to dynamic flight measurements.
7. J. NASIR and S. S. SUNDER 1982 *Research Report R* 82-52, *Department of Civil Engineering*, *Massachussets Institute of Technology*. An evaluation of the random decrement technique of vibration signature analysis for monitoring of offshore platforms.
8. J. C. ASMUSSEN, S. R. IBRAHIM and R. BRINCKER 1996 *Proceedings of* 14*th International Modal Analysis Conference*, *Dearborn*, *MI*, 453–458. Random decrement and regression analysis of traffic responses of bridges.
9. J. C. ASMUSSEN, S. R. IBRAHIM and R. BRINCKER 1998 *Proceedings of* 16*th International Modal Analysis Conference*, *Santa Barbara*, *CA*, 914–921. Random decrement: identification of structures subjected to ambient excitation.
10. C. B. YUN and E. Y. BAHNG 1999 *Computer and Structures* **77**, 41–52. Substructural identification using neural networks.
11. C. B. YUN, J. H. YI and E. Y. BAHNG 2001 *Engineering Structures* **23**, 425–435. Joint damage assessment of framed structures using neural networks technique.
12. K. MATSUOKA 1992 *IEEE Transactions on Systems*, *Man and Cybernetics* **22**, 436–440. Noise injection into inputs in back-propagation.
13. C. B. YUN, E. Y. BAHNG and J. H. YI 1998 *Proceedings of Structural Engineers World Congress*, *San Francisco*, *CA*. Neural network approach to damage assessment of civil structures.
14. D. F. MAZUREK and J. T. DEWOLF 1990 *Journal of Structural Engineering American Society of Civil Engineers* **116**, 2532–2549. Experimental study of bridge monitoring technique.
15. W. PRESS, S. A. TEUKOLSKY, W. T. VETTERLING and B. P. FLANNERY 1992 *Numerical Recipes in C—the Art of Scientific Computing*. New York: Cambridge University Press.
16. V. N. VAPNIK and A. Y. CHERVONENKIS 1971 *Theory of Probability and its Applications* **16**, 264–280. On the uniform convergence of relative frequencies of events to their probabilities.

APPENDIX A

To investigate the effect of the vehicle speed on the operational modal properties, preliminary tests were carried out on the bridge model with smaller girders (H—$50 \times 50 \times 4{\cdot}5 \times 4{\cdot}5$) for speeds of 2·0, 2·5, and 3·0 m/s with one test vehicle (60 kgf). The corresponding speeds for the prototype cases are 36·1, 45·1, and 54·1 km/h. The properties of the operational modes were estimated for each speed for the four lowest modes, and the results are summarized in Tables A1 and A2.

TABLE A1

Resonant frequencies (f_m) *for each speed* (Hz)

Modes	$V_m = 2{\cdot}0$ m/s $V_p = 36{\cdot}1$ m/s	$V_m = 2{\cdot}5$ m/s $V_p = 45{\cdot}1$ m/s	$V_m = 3{\cdot}0$ m/s $V_p = 54{\cdot}1$ m/s
1	5·82	5·81	5·85
2	16·43	16·43	16·45
3	35·06	35·03	35·02
4	58·32	58·30	58·28

TABLE A2

Modal assurance criteria for cases with two vehicle speeds

Modes	$V_m = 2{\cdot}0$ and $2{\cdot}5$ m/s	$V_m = 2{\cdot}0$ and $3{\cdot}0$ m/s	$V_m = 2{\cdot}5$ and $3{\cdot}0$ m/s
1	0·9995	0·9996	0·9987
2	0·9996	0·9991	0·9994
3	0·9992	0·9997	0·9994
4	0·9982	0·9911	0·9966